Organic Electronics 73 (2019) 212–218

Contents lists available at ScienceDirect

Organic Electronics

journal homepage: www.elsevier.com/locate/orgel

Control of morphological and electrical properties of flexographic printed electronics through tailored ink rheology

Miles L. Morgan[a], Dan J. Curtis[b], Davide Deganello[a,*]

[a] Welsh Centre for Printing and Coating, College of Engineering, Swansea University, Swansea, SA1 8EN, United Kingdom
[b] Complex Fluids Research Group, College of Engineering, Swansea University, Swansea, SA1 8EN, United Kingdom

ARTICLE INFO

Keywords:
Flexography
Rheology
Printed electronics
Extensional flow
Elasticity

ABSTRACT

Functional model inks were formulated and printed using flexography in order to assess the influence of ink extensional elasticity and print velocity on the morphological and electrical properties of printed layers. Increased extensional elasticity and higher print velocity resulted in the printing of more isotropic prints, both morphologically and electronically. Furthermore, a correlation between the prints' morphological and electrical anisotropy strongly suggests that print uniformity has a considerable influence on functionality and that ink rheology may be used to control such characteristics.

1. Introduction

Flexography is a roll-to-roll printing process that is well-established in the packaging industry and capable of high speed, patterned deposition of fluids of a range of viscosities [1]. As such, the technique is considered to have tremendous potential in the mass-production of printed electronic devices. Conductive grids [2], transistors [3], biosensors [4] and photovoltaics [5,6] all have been fabricated using flexography. Furthermore, this low-waste process can be performed at ambient temperature with flexible substrates. However, unlike the more subjective nature of graphical print applications, prints for electronics purposes have a greater requirement for good print uniformity. Poor uniformity will limit the conductivity of a print leading to functional variation and short circuits in multi-layered devices. Understanding the causes of such non-uniformity is therefore of considerable interest so that they may be controlled and even exploited.

A common cause of non-uniformity in flexographic printing is the phenomenon of "viscous fingering", sometimes referred to as ribbing [7–10]. Viscous fingering has been attributed to the Saffman-Taylor instability that occurs when a less viscous fluid displaces a more viscous fluid [11]. In the context of flexographic printing it is thought that viscous fingering occurs as the ink is split after the nip between the printing plate and the freshly inked substrate, as illustrated in Fig. 1.

Their separation creates a dynamic meniscus between air and the ink which is subjected to both shear and extensional stresses [7]. Competition between viscous and surface tension forces typically leads to the formation of fingers with a characteristic wavelength which decreases with the dimensionless capillary number $Ca = \eta v/\sigma$ (where v is printing velocity and η and σ are fluid shear viscosity and surface tension, respectively) [7,12]. However, this parameter does not consider viscoelastic fluid properties which are often displayed in functional printing inks (that typically contain significant amounts of polymer binder and solid particles of various shapes and sizes). The Deborah number, defined as the ratio of the material relaxation time λ and the characteristic time scale of the flow T is often used to characterise viscoelasticity in complex flows [13]. In the present context, T may be described in terms of v and ink thickness at the nip l [14,15]:

$$De = \frac{\lambda}{T} = \frac{\lambda v}{l} \quad (1)$$

While work has been done concerning instabilities including ribbing and filamentation in other roller processes such as forward roll coating [16–18], little has focussed on their occurrence in flexography. Some analysis has been carried out with respect to the wavelength of the features across the print [8,12] but this does not consider how such features evolve in the printing direction. This may be of particular interest as ribs in forward roll coating become unsteady as Ca is increased resulting in oscillation, wandering and merging while evolving into septa downstream [19,20]. Recently it was reported that features induced by instabilities in flexography became significantly smaller with increased ink elasticity. This effect can be linked to filamentation [21] - a phenomenon characteristic of the extensional flows that are often observed in roller processes [17,22]. Resultant prints can therefore exhibit various morphologies including continuous stripes, branching

* Corresponding author.
E-mail address: D.Deganello@swansea.ac.uk (D. Deganello).

https://doi.org/10.1016/j.orgel.2019.05.027
Received 15 April 2019; Received in revised form 14 May 2019; Accepted 14 May 2019
Available online 22 May 2019

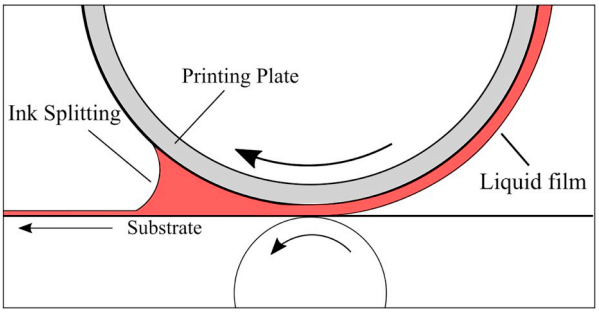

Fig. 1. Illustration of ink splitting in flexography as the printing plate and the substrate are separated.

and dotting [21]. Direct relation of such morphological phenomena to electrical performance has not been carried out, although feature size and orientation is likely to have a considerable effect in this regard.

Herein, a set of printable, conductive fluids were formulated that display identical rheological properties under shear but with markedly different behaviour in extensional flow. As such, the influence of ink extensional properties and printing velocity on the uniformity and subsequent functionality of prints was isolated and examined.

2. Experimental

2.1. Ink formulation

Model inks were formulated by modifying the printable elastic fluids of Morgan et al. [21] with the addition of a poly(3,4-ethylenedioxythiophene) polystyrene sulfonate (PEDOT:PSS) solution to provide electrical conductivity. Solutions of polyvinyl alcohol (PVA) of molecular weight $20–30 \times 10^3$ g/mol and degree of hydrolysis 88% (Acros Organics) in deionised water were mixed with a water-based Orgacon PEDOT:PSS solution by Agfa (modified S305 with 1.7 wt% PEDOT:PSS) before the addition of aqueous E122 azorubine dye (FastColors LLP) to highlight printed patterns and polyacrylamide (PAM) of molecular weight 5–6 x 10^6 g/mol (Acros Organics) in deionised water to provide extensional elasticity. The respective compatibility of PVA and PAM with PEDOT:PSS is well-documented [23–25] and the present formulations combine the properties of each in a flexographically printable set of fluids. The contents of the three inks formulated are shown in Table 1. When dried, a solid film of each ink therefore contained 38.7 wt% PEDOT:PSS.

2.2. Ink characterisation

Apparent shear viscosity was measured using a Malvern Bohlin Gemini HR Nano rheometer with a 40 mm, 4° stainless steel cone and plate geometry between shear rates of 0.1 and 100 s^{-1}. Small amplitude oscillatory shear (SAOS) measurements were performed using a TA Instruments AR-G2 rheometer with a 60 mm aluminium parallel plate geometry and a gap of 350 μm. Frequency sweeps were carried out at a constant stress of 0.2 Pa which was within the linear viscoelastic region of all inks. All measurements were performed at 20 °C. Due to the extensional flows present in roller processes, a custom built capillary breakup extensional rheometer (CaBER) was used to characterise the uniaxial extensional properties of the inks. CaBER has been utilised for the characterisation of fluids in a range of applications including roller processing [26], drag reduction [27] and electrospinning [28]. In this method a small volume of fluid is loaded between two plates that are then separated in a step strain causing a liquid filament to form and subsequently break under capillary, viscous and/or elastic stresses [29]. By monitoring the evolution of the capillary midfilament diameter $D_{mid}(t)$ with time this technique enables the calculation of extensional viscosity as

$$\eta_E = (2X - 1)\frac{\sigma}{-dD_{mid}/dt} \tag{2}$$

where σ is the ink surface tension and X is a dimensionless variable dependent on the tensile force and radius of the filament [30]. X is taken to be 0.7127 for Newtonian fluid breakup [31] while for elastic breakup $X = 1$ due to the axial symmetry of the filament [32]. Idealised elastic filament breakup may be modelled as

$$\frac{D_{mid}(t)}{D_1} = \exp(-t/3\lambda_E) \tag{3}$$

where D_1 is mid-filament diameter just after extension, t is time and λ_E is the fluid's characteristic relaxation time for the elastocapillary thinning action [33]. A plate diameter of 3 mm was used for the CaBER experiments and filament breakup was filmed using a FastCam Mini high speed camera at frame rates between 1000 and 4000 frames per second.

Ink density was determined with a pycnometer and surface tension using a pendant drop method [34] with images taken using the FastCam camera and analysed with ImageJ software [35].

2.3. Flexographic printing and uniformity analysis

Inks were printed on 250 μm polyethylene terephthalate (PET) with an IGT F1 Printability Tester. Printing and anilox forces of 50 N were used with print velocities of 0.2, 0.6 and 1.0 m/s and a 24 cm^3/m^2 anilox. Solid area, 100% nominal coverage printing plates consisting of a 3 cm wide strip were selected to assist in the analysis of print uniformity. After drying at room temperature, the prints were cut to 20 × 20 mm squares and digitised with an Epson Perfection V700 scanner at 2000 dots per inch. Areas of each scan 1260 × 1260 pixels in size (16 × 16 mm) were used for morphological analysis which was performed using Wolfram Mathematica [36] as follows.

A two dimensional approach was employed in the characterisation of print uniformity which is illustrated in Fig. 2. Digitised images were binarised with the threshold determined using Otsu's method [37] before being subjected to a median filter with a radius of 1 pixel (12.7 μm) to suppress the influence of noise whilst retaining the features of interest. Transitions from black to white pixels were counted along each row (x-direction) and down each column (y-direction) before their respective means were calculated. These quantities, once scaled according to the image resolution, therefore represent twice the average wavenumber k of the ink features in each direction. Hence, the wavenumbers k_x and k_y describe the general spatial frequency of the undulations on the print perpendicular and parallel to the printing direction respectively. The ratio k_y/k_x therefore characterises the print anisotropy. For instance, a morphologically isotropic print will have $k_y/k_x = 1$, while for long features in the printing direction $k_y/k_x < 1$.

2.4. Electrical characterisation

Due to the typical size of the morphological features and their varying anisotropic nature, four-point probe testing was not suitable as the probe size and inter-probe distance were the same order of size as the morphological features of interest. As such, a custom probe was fabricated consisting of two copper strips 16 mm long and 450 μm thick fixed 16 mm apart as pictured in Fig. 3. The resistance of each print square was measured both perpendicular and parallel to the printing

Table 1
Solid weight contents of formulated inks.

Ink	PEDOT:PSS (wt%)	PVA (wt%)	PAM (wt%)	Dye (wt%)
P0	1.09	1.625	0	0.1
P1	1.09	1.6125	0.0125	0.1
P2	1.09	1.6	0.025	0.1

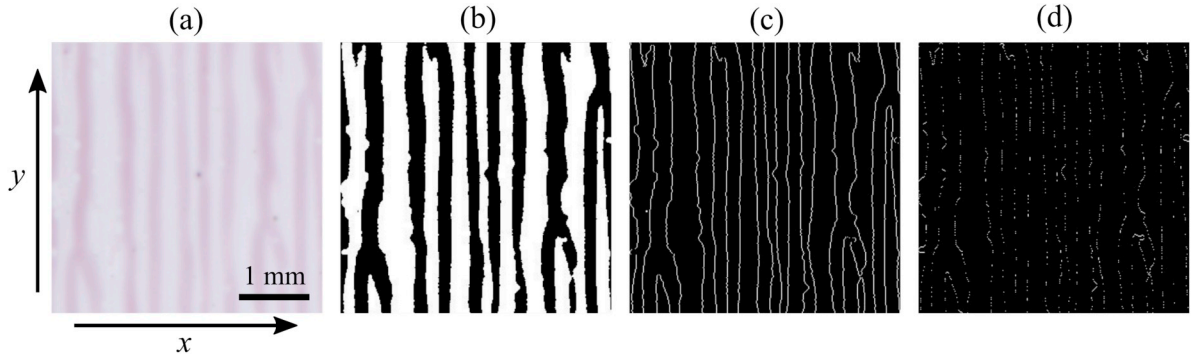

Fig. 2. (a) A print area that has been (b) binarised and subjected to feature analysis in the (c) *x*- and (d) *y*-direction.

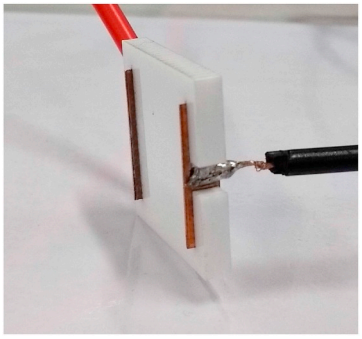

Fig. 3. Directional resistance probe.

direction and a load of 0.18 N was applied to the contacts to ensure consistent probe-sample contact. The resistance between the copper strips was recorded as R_x and R_y (perpendicular and parallel to the printing direction, respectively) and the ratio R_y/R_x was calculated as a measure of electrical anisotropy. This technique was able to provide a repeatable measure of the prints' electrical performance and a direct directional comparison, despite the presence of exaggerated non-uniformity. Characterisation of print samples was carried out in a temperature-controlled room (20 ± 1°C /~40% RH).

In order to confirm that each ink displayed identical electrical properties, an RK Print Coat Instruments K Control Coater was used to bar coat 250 µm PET with a nominally 12 µm thick layer of ink (this being comparable to the print thickness achieved from the anilox volume employed herein [38]). After drying, the samples were cut into 18.75 × 18.75 mm squares and their sheet resistance was measured using a four-point probe [39]. Optical density measurements of these coated samples were performed using a Spectrolino by Gretag Macbeth.

3. Results and discussion

3.1. Ink characterisation

The apparent viscosity, η, of each ink as a function of shear rate is shown in Fig. 4. All inks show mild shear thinning properties with η decreasing from approximately 0.1 Pa·s to about 0.03 Pa·s over three orders of shear rate. This is qualitatively typical of aqueous PEDOT:PSS solutions [40]. Notably, all three inks exhibit near identical shear viscosity profiles. Elastic and viscous moduli, G' and G'' respectively, are shown as a function of frequency in Fig. 5 for all inks. The similarity of G'' for each formulation is consistent with the viscosity measurements of Fig. 4. Interestingly, G' is also similar between inks, in contrast to measurements of PVA/PAM blends that show increasing G' with PAM content [21]. Furthermore, G' measurements for the present inks are an order of magnitude higher than those seen by Morgan et al. [21], suggesting that PEDOT:PSS, not PVA or PAM, is the main contributor to the shear elasticity.

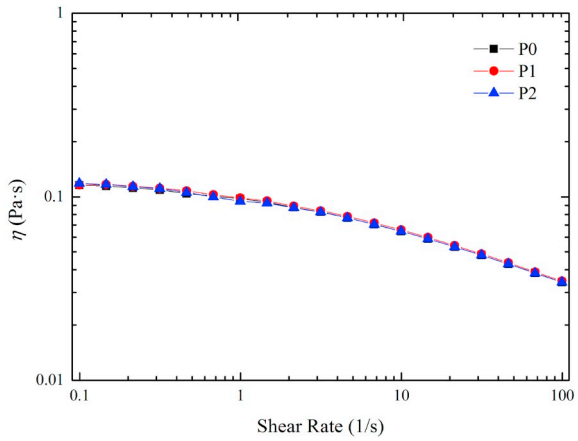

Fig. 4. Apparent viscosity η with shear rate for all inks.

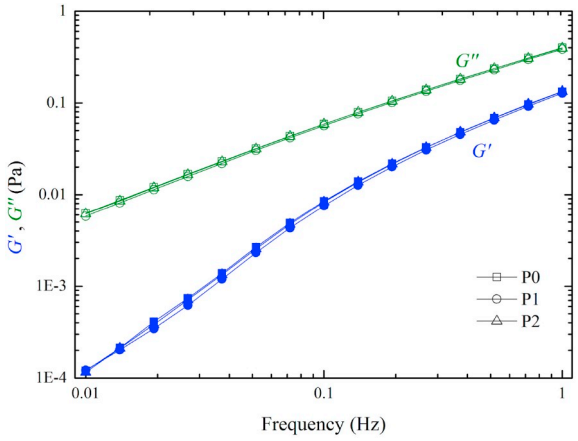

Fig. 5. Typical G' (filled symbols) and G'' (unfilled symbols) with frequency for all inks.

Midfilament diameter profiles from extensional rheometry measurements are shown in Fig. 6. Breakup times increase considerably with PAM content and the PAM-containing inks both show exponential decay which is characteristic of elastic behaviour [29]. After an initial retardation, likely due to gravitational drainage, filament breakup of ink P0 becomes more linear, with fitting of equation (2) revealing an extensional viscosity $\eta_E = 0.18 \pm 0.01$ Pa·s. This is not inconsistent with the Trouton ratio $\eta_E = 3\eta$ for Newtonian fluids [41], considering the viscosity range shown in Fig. 4, suggesting inelastic behaviour in extension. The extensional relaxation times of inks P1 and P2, determined by fitting equation (3) to the elasto-capillary regime of filament breakup, are shown in Table 2 and increase considerably with PAM

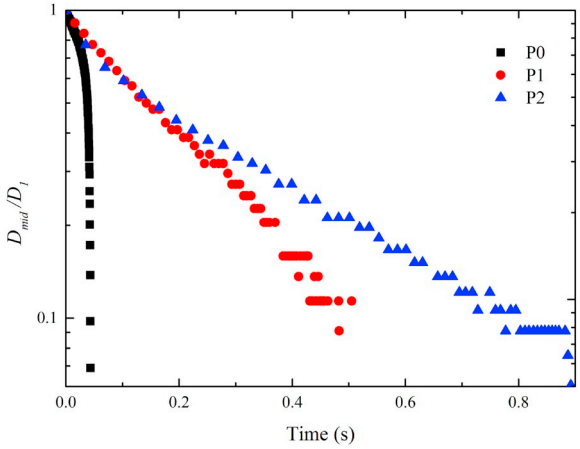

Fig. 6. Typical normalised CaBER filament diameter with time for each ink.

content. Furthermore, Fig. 7 shows filaments observed during CaBER for inks P0 and P2. The curvature of that formed from ink P0 is consistent with Newtonian behaviour and the slender, cylindrical nature of P2 is characteristic of extensionally elastic fluids [32]. While the viscous and elastic behaviour in shear is very similar for all three inks, the elasticity under extensional flow conditions varies substantially. This novel class of fluids therefore allows for the isolation and analysis of effects related to extensional flows in complex processes.

3.2. Print uniformity analysis

Print samples for the three inks printed at three different velocities are shown in Fig. 8 with non-uniformity akin to viscous fingering being displayed in all prints. The extensionally inelastic ink, P0 exhibits a near-continuous striping in the printing direction at 0.2 and 0.6 m/s. This characteristic is disrupted with increased λ_E, possibly as a consequence of increased wandering and merging of ribs. This is consistent with the convergence of the fingers in the printing direction. An apparent increase in the prevalence of darker dots as λ_E is increased suggests filamentation is also occurring, which has been previously observed in elastic inks due to the rupture of advanced ribs [22]. Increasing v appears to result in a more branched morphology, with further disruption of the longer, striped features. This behaviour was quantified by calculating the average wavenumbers k_x and k_y and the ratio between them k_y/k_x which is plotted in Fig. 9(a) as a function of λ_E, with λ_E of ink P0 taken to be zero. As k_y/k_x is always less than 1, $k_x > k_y$ confirming the finger-like features are oriented in the printing direction. The ratio is seen to increase with increasing λ_E and v signifying a more isotropic morphology. These phenomena can be confirmed by visual inspection of the prints and may be attributed to a significant increase in surface undulation in the y-direction as k_x decreased only slightly with v and λ_E. Error bars on Fig. 9(a) represent standard deviations of different print samples which are considerable for P0 at the highest velocity. However, as the extensional elasticity is increased the variation between prints at this velocity is reduced, suggesting a more repeatable print outcome was achieved.

The aforementioned Deborah number De may be employed to consolidate the variables v and λ_E and is used to plot k_y/k_x in Fig. 9(b)

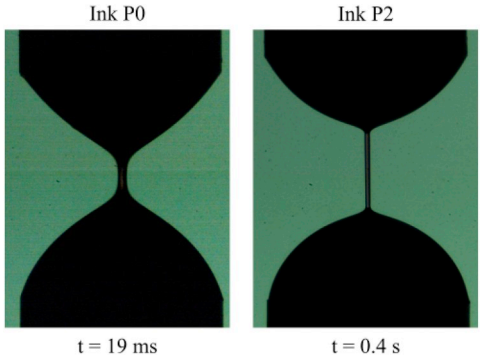

Fig. 7. Images of filamentation in CaBER for inks P0 and P2 at similar $D_{mid}(t)$.

for all non-zero values of De (inks P1 and P2). The wavenumber ratio, and therefore print isotropy, increases with De. Furthermore, the data collapse to a single linear line, highlighting the strong relation between ink extensional elasticity, print velocity and print isotropy. This is of particular interest with regards to the tailoring of ink rheology for desired printed patterns.

3.3. Electrical characterisation

The sheet resistance R_s of the bar-coated samples of each ink is displayed in Table 2. All three inks have similar sheet resistances although a slight increase is seen with PAM content. This is thought to be due to a minor difference in coated layer thickness rather than detrimental effects of PAM addition, a notion supported by optical density measurements given in Table 2 that show a decrease with PAM content.

Apparent print resistance, measured in the x- and y-directions is displayed in Fig. 10(a) and (b) respectively as a function of λ_E. Notably, contact resistance between the probe and print surface, determined by transfer line measurement, was found to be ~2 kΩ - an order of magnitude smaller than the lowest sample values.

Print velocity appears to have a significant influence on print resistance in each direction, with increasing v resulting in a decrease of both R_x and R_y. This is possibly due to the shear thinning nature of the inks facilitating transfer at higher speeds and enabling the deposition of a thicker layer. A general reduction in R_x occurs with λ_E, shown in Fig. 10(a), which coincides with the apparent increase in branching in the x-direction. This is particularly apparent at 0.2 m/s, where R_x is reduced by an order of magnitude as λ_E is increased from 0 to 133 ms. Along the prints, as seen in Fig. 10(b), λ_E has a less conclusive impact except at 0.2 m/s, where R_y increases by a factor of four from inks P0 ($\lambda_E = 0$ ms) to P1 ($\lambda_E = 78$ ms). It is possible that disruption of the continuous morphological features resulted in a more electrically resistive path in the y-direction.

The ratio R_y/R_x provides a comparison of the electrical performance in each direction and is shown as a function of λ_E in Fig. 11(a). As both λ_E and v are increased R_y/R_x increases closer to unity suggesting more isotropic electrical properties. In the most extreme case of electrical anisotropy, the extensionally inelastic P0 at the lowest print velocity, the resistance across the print R_x is about 300 times that of the resistance along it, R_y. This print also has the lowest k_y/k_x and is therefore the most morphologically anisotropic. R_y/R_x is plotted with the non-

Table 2
Properties of the formulated inks: surface tension (σ), shear viscosity (η) at 1 s^{-1}, elastic modulus (G') at 1 Hz and extensional relaxation time (λ_E) in addition to sheet resistance (R_s) and optical density (OD) of bar coated samples.

Ink	σ (mN/m)	η (mPa·s)	G' (Pa)	λ_E (ms)	R_s (kΩ/□)	OD
P0	42.8 ± 1.5	99.0 ± 1.7	0.133 ± 0.002	–	0.57 ± 0.03	0.340 ± 0.004
P1	43.4 ± 2.5	98.6 ± 1.9	0.128 ± 0.001	78 ± 4	0.59 ± 0.02	0.323 ± 0.007
P2	42.9 ± 2.0	97.3 ± 2.2	0.138 ± 0.007	133 ± 4	0.64 ± 0.02	0.312 ± 0.003

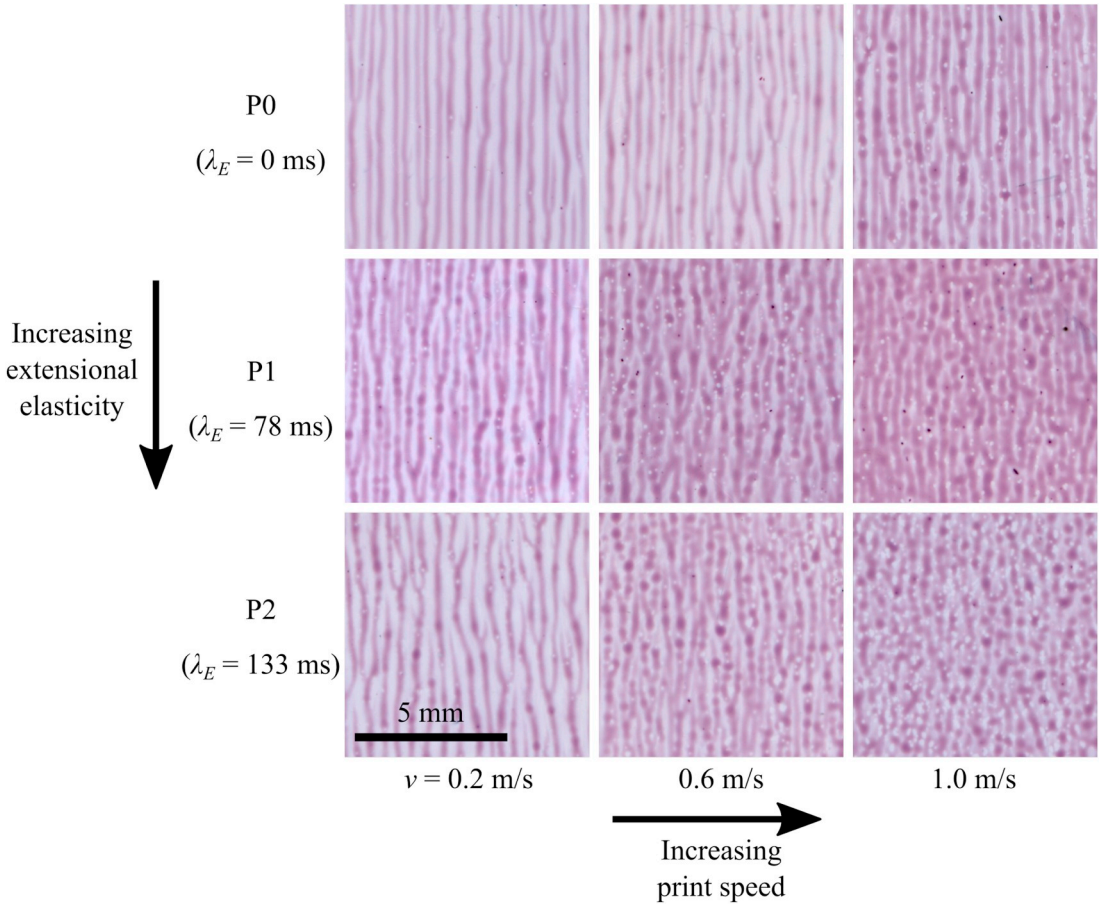

Fig. 8. Print samples of the three inks at each printing velocity with brightness adjusted for visual representation.

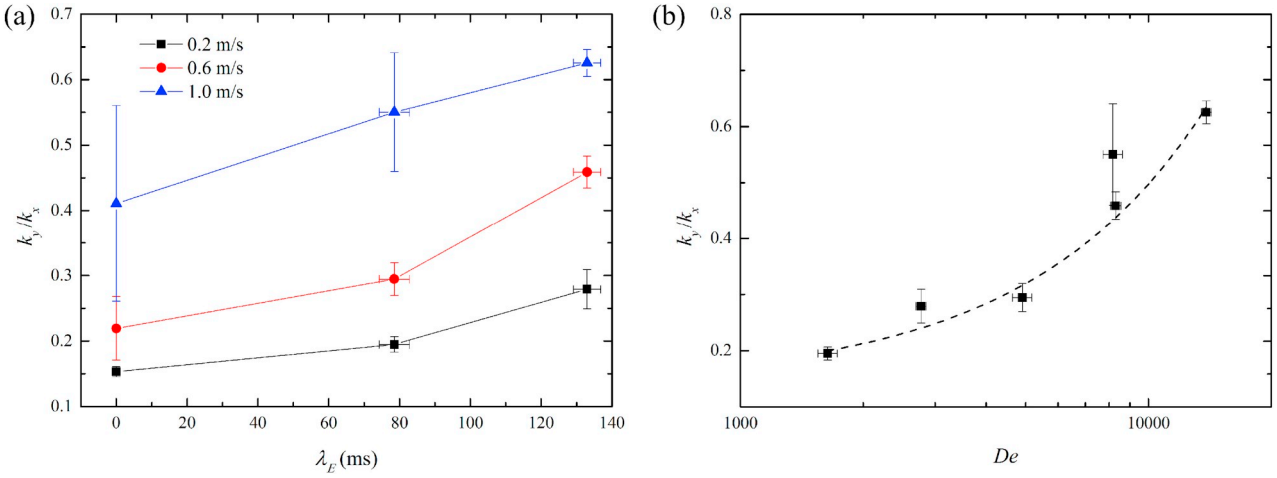

Fig. 9. Morphological wavenumber ratio k_y/k_x plotted with (a) extensional relaxation time λ_E and (b) Deborah number *De*.

zero Deborah numbers in Fig. 11(b) where the data collapse to a linear line suggesting rheological correlation with electrical print performance. This is a significant result regarding the optimisation of device functionality through ink rheology and even indicates that printing instabilities may be used as a low-cost, scalable means of obtaining anisotropic conductive layers.

3.4. Morhpological vs electrical properties

The previously defined ratios k_y/k_x and R_y/R_x provide measures of the morphological and electrical anisotropy of the prints and are plotted together in Fig. 12. They exhibit a generally linear relationship with a gradient of approximately 1, showing a clear relation between the orientation of printed patterns and directional electrical performance. As the wavenumber ratio k_y/k_x approaches unity - signifying a more isotropic morphology - so too does the electrical resistance ratio R_y/R_x. This suggests the orientation of printed features, in this case non-uniformity caused by surface instabilities, has a direct link to the resistance of a print in a given direction. Ink rheology and process parameters have therefore been used to control the nature of printed

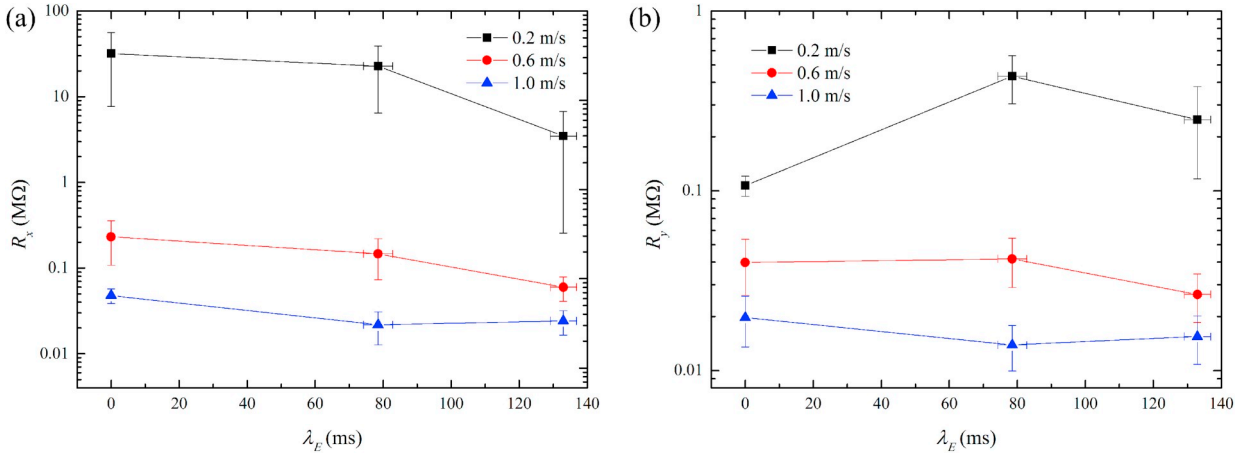

Fig. 10. Resistance measured (a) in the *x*-direction and (b) in the *y*-direction with extensional relaxation time λ_E.

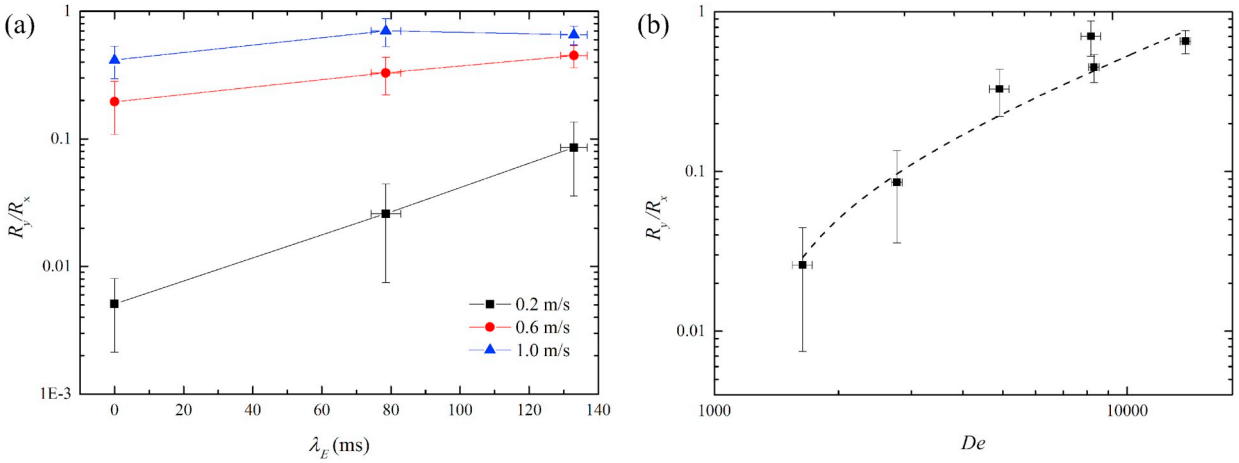

Fig. 11. Resistance ratio R_y/R_x with (a) extensional relaxation time λ_E and (b) Deborah number *De*.

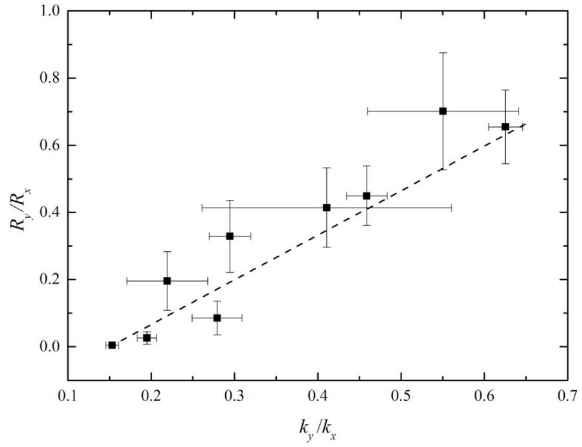

Fig. 12. Resistance ratio R_y/R_x against morphological wavenumber ratio k_y/k_x.

patterns which have in turn dictated the prints' directional electrical performance. This presents a new way of obtaining specific printed patterns and control of print functionality.

4. Conclusions

Conductive model rheological inks were formulated to assess the influence of ink rheology on functional print performance. These inks behaved similarly in shear flow but were markedly different in extension, displaying varying degrees of extensional elasticity. When flexographically printed, viscous fingering oriented in the printing direction was observed on all prints. Concurrently, prints were found to be more electrically conductive in the direction of the finger-like features. As ink extensional elasticity and print velocity increased these features became less continuous and the prints became morphologically more isotropic. This was further reflected in the electrical behaviour, with resistance measured along and across the prints becoming more alike. While control was obtained over the nature of the printed patterns, the inhomogeneities were not eliminated altogether. Future work to achieve smooth, uniform layers may hence consider probing wider ranges of the capillary and Deborah numbers or additional treatments of the substrate, plate and prints.

Ink rheology has therefore been shown to influence not only the morphological nature of flexographic prints, but also their functional performance. This emphasises the importance of rheology in functional printing and advances the prospect of tailoring ink rheology for desired print properties.

Acknowledgements

This work was supported by the EPSRC (UK) grant number EP/M008827/1.

References

[1] H. Kipphan, Handbook of Print Media: Technologies and Production Methods, Springer, 2001.

[2] D. Deganello, J.A. Cherry, D.T. Gethin, T.C. Claypole, Impact of metered ink volume on reel-to-reel flexographic printed conductive networks for enhanced thin film conductivity, Thin Solid Films 520 (2010) 2233–2237.
[3] H. Yan, Z. Chen, Y. Zheng, C. Newman, J.R. Quinn, F. Dötz, M. Kastler, A. Facchetti, A high-mobility electron-transporting polymer for printed transistors, Nature 457 (2009) 679–687.
[4] J. Benson, C.M. Fung, J.S. Lloyd, D. Deganello, N. Smith, K.S. Teng, Direct patterning of gold nanoparticles using flexographic printing for biosensing applications, Nanoscale Res. Lett. 10 (2015) 127.
[5] S. Alem, N. Graddage, J. Lu, T. Kololuoma, R. Movileanu, Y. Tao, Flexographic printing of polycarbazole-based inverted solar cells, Org. Electron. 52 (2018) 146–152.
[6] J. Baker, D. Deganello, D. Gethin, T. Watson, Flexographic printing of graphene nanoplatelet ink to replace platinum as counter electrode catalyst in flexible dye sensitised solar cell, Mater. Res. Innov. 18 (2) (2014) 86–90.
[7] H.M. Sauer, N. Bornemann, E. Dörsam, Viscous fingering in functional flexo printing: an inevitable bug? Proceedings of the Large-Area, Organic and Printed Electronics Convention (LOPE-C), 2011.
[8] H.M. Sauer, D. Daume, E. Dörsam, Lubrication theory of ink hydrodynamics in the flexographic printing nip, J. Print Media Technol. 4 (3) (2015) 163–172.
[9] M. Hösel, F.C. Krebs, Large-scale roll-to-roll photonic sintering of flexo printed silver nanoparticle electrodes, J. Mater. Chem. 22 (31) (2012) 15683–15688.
[10] Z. Wang, R. Winslow, D. Madan, P.K. Wright, J.W. Evans, M. Keif, X. Rong, Development of MnO2 cathode inks for flexographically printed rechargeable zinc-based battery, J. Power Sources 268 (2014) 246–254.
[11] P. Saffman, G. Taylor, The penetration of a fluid into a porous medium or Hele-Shaw cell containing a more viscous liquid, Proc. R. Soc. A 245 (1958) 312–329.
[12] C. Voß, Analytische modellierung, experimentelle untersuchungen und dreidimensionale gitter-boltzmann-simulation der quasistatischen und instabilen farbspaltung, Ph.D. thesis Bergische Universitt Gesamthochschule Wuppertal, 2002.
[13] M. Reiner, The Deborah Number, Phys. Today 17 (1964) 62.
[14] R. Bird, W. Stewart, E. Lightfoot, D. Klingenberg, Introductory Transport Phenomena, John Wiley and Sons Ltd, 2015.
[15] H.A. Lécuyer, J.P. Mmbaga, R.E. Hayes, F.H. Bertrand, P.A. Tanguy, Modelling of forward roll coating flows with a deformable roll: application to non-Newtonian industrial coating formulations, Comput. Chem. Eng. 33 (9) (2009) 1427–1437.
[16] J.R.A. Pearson, The instability of uniform viscous flow under rollers and spreaders, J. Fluid Mech. 7 (4) (1960) 481–500.
[17] R.H. Fernando, J.E. Glass, Dynamic uniaxial extensional viscosity (DUEV) effects in roll application II: polymer blend studies, J. Rheol. 32 (2) (1988) 199–213.
[18] G.A. Zevallos, M.S. Carvalho, M. Pasquali, Forward roll coating flows of viscoelastic liquids, J. Non-Newtonian Fluid Mech. 130 (2005) 96–109.
[19] M.S. Owens, M. Vinjamur, L.E. Scriven, C.W. Macosko, Misting of Newtonian liquids in forward roll coating, Ind. Eng. Chem. Res. 50 (6) (2011) 3212–3219.
[20] E. Pitts, J. Greiller, The flow of thin liquid films between rollers, J. Fluid Mech. 11 (1) (1961) 33–50.
[21] M.L. Morgan, A. Holder, D.J. Curtis, D. Deganello, Formulation, characterisation and flexographic printing of novel Boger fluids to assess the effects of ink elasticity on print uniformity, Rheol. Acta 57 (2) (2018) 105–112.
[22] M.S. Owens, M. Vinjamur, L. Scriven, C. Macosko, Misting of non-Newtonian liquids in forward roll coating, J. Non-Newtonian Fluid Mech. 166 (19–20) (2011) 1123–1128.
[23] O. Carr, G. Gozzi, L.F. Santos, R.M. Faria, D.L. Chinaglia, Analysis of the electrical and optical properties of PEDOT:PSS/PVA blends for low-cost and high-performance organic electronic and optoelectronic devices, Transl. Mater. Res. 2 (1) (2015) 015002.
[24] C.H. Chen, A. Torrents, L. Kulinsky, R.D. Nelson, M.J. Madou, L. Valdevit, J.C. Larue, Mechanical characterizations of cast Poly(3,4-ethylenedioxythiophene): poly(styrenesulfonate)/Polyvinyl Alcohol thin films, Synth. Met. 161 (21–22) (2011) 2259–2267.
[25] F.A. Aouada, M.R. Guilherme, G.M. Campese, E.M. Girotto, A.F. Rubira, E.C. Muniz, Electrochemical and mechanical properties of hydrogels based on conductive poly (3,4-ethylene dioxythiophene)/poly(styrenesulfonate) and PAAm, Polym. Test. 25 (2) (2006) 158–165.
[26] S. Khandavalli, J.P. Rothstein, Ink transfer of non-Newtonian fluids from an idealized gravure cell: the effect of shear and extensional deformation, J. Non-Newtonian Fluid Mech. 243 (2017) 16–26.
[27] B.E. Owolabi, D.J.C. Dennis, R.J. Poole, Turbulent drag reduction by polymer additives in parallel-shear flows, J. Fluid Mech. 827 (2017) R4.
[28] J.H. Yu, S.V. Fridrikh, G.C. Rutledge, The role of elasticity in the formation of electrospun fibers, Polymer 47 (2006) 4789–4797.
[29] G.H. Mckinley, Visco-elasto-capillary thinning and break-up of complex fluids, Annual Rheology Reviews 3 (2005) 1–49.
[30] T.R. Tuladhar, M.R. Mackley, Filament stretching rheometry and break-up behaviour of low viscosity polymer solutions and inkjet fluids, J. Non-Newtonian Fluid Mech. 148 (2008) 97–108.
[31] D.T. Papageorgiou, On the breakup of viscous liquid threads, Phys. Fluids 7 (1995) 1529–1544.
[32] G.H. McKinley, A. Tripathi, How to extract the Newtonian viscosity from capillary breakup measurements in a filament rheometer, J. Rheol. 44 (2000) 653–670.
[33] A.V. Bazilevsky, V.M. Entov, A.N. Rozhkov, Liquid filament microrheometer and some of its applications, Proceedings of Third European Rheology Conference and Golden Jubilee Meeting of the British Society of Rheology (1990) 41–43.
[34] R.M. Bidwell, J.L. Duran, G.L. Hubbard, Tables for the Determinaton of the Surface Tensions of Liquid Metals by the Pendant Drop Method, University of California Los Alamos Scientific Laboratory, 1964, pp. 1–11.
[35] C.A. Schneider, W.S. Rasband, K.W. Eliceiri, NIH Image to ImageJ : 25 years of image analysis, Nat. Methods 9 (7) (2012) 671–675.
[36] Wolfram Research, Inc., Mathematica Version 10.1, (2015).
[37] N. Otsu, A threshold selection method from gray-level histograms, IEEE Transactions on Systems Man Cybernet SMC- 9 (1) (1979) 62–66.
[38] J.A. Cherry, Ink Release Characteristics of Anilox Rolls, Ph.D. thesis University of Wales Swansea, 2007.
[39] F.M. Smits, Measurement of sheet resistivities with the fourpoint probe, Bell System Technical J. 37 (3) (1958) 711–718.
[40] R.P. Raja Ashok, M.S. Thomas, S. Varughese, Multi-region to single region shear thinning transitions in drying PEDOT:PSS dispersions: contributions from charge density fluctuations, Soft Matter 11 (43) (2015) 8441–8451.
[41] H.A. Barnes, J.F. Hutton, K. Walters, An Introduction to Rheology, Elsevier Science Publishers B.V., 1989.